Available online at www.elixirpublishers.com (Elixir International Journal)

Electrical Engineering

Elixir Elec. Engg. 75 (2014) 27568-27574

ISSN: 2229-712X

Sensor less torque and speed control of five level converters for AC drive using SVPWM technique

G. Chakradhara Rao[1*], K.Sravanthi[2], K. Durga Syam Prasadi[3] and K.Vijay Kumar[4]

[1]Department of EEE, DIET College of Engineering, Visakhapatnam- 531 002.

[2]Department of EEE, Vignan's Institute of Information Technology, Visakhapatnam.

[3]Department of EEE, DIET College of Engineering, Visakhapatnam- 531 002.

[4]Department of EEE, DIET's Institute of Engineering, Visakhapatnam- 531 002.

ARTICLE INFO

Article history:

Received: 16 July 2014;

Received in revised form:

20 September 2014;

Accepted: 4 October 2014;

Keywords

Direct torque control,

Space vector Pulse width Modulation (SVPWM),

Neutral point clamped (NPC),

Two-level inverter,

AC–AC conversion, Control strategies,

Matrix converter (MC), EKF,

Modulation schemes.

ABSTRACT–

Various applications, like in underground mines and oil and gas industries, require remote operation of vector-controlled medium-voltage variable speed drives via a long motor feeder. The use of voltage source inverters in such cases leads to motor overvoltage and harmonic quality problems. The current source inverter (CSI) is ideally matched to these applications be-cause of its motor-friendly voltage output. Speed sensorless operation is mandatory due to the long motor feeder. Although the model reference adaptive system (MRAS) is a powerful and proven speed estimation tool, its implementation in long motor feeder drives faces many challenges. Among them, and addressed in this paper, are inherent dc offset in its stator model, the need for actual motor voltage and current values, and oscillations in the estimated speed due to errors in the motor current measurement signals. In this paper, a sensorless CSI vector-controlled drive, suitable for long motor feeder applications, is studied. Improved speed estimation is achieved by proposing 1) a modified dc-offset eliminator for an MRAS speed estimation and 2) a compensation technique for mo-tor current's measurement errors. Intensive experimental results, for a low-voltage scaled model, along with simulations validate the effectiveness of the proposed technique. In this Proposed Control technique of the space vector modulation Technique (SVPWM) is applied to 5 level inverter controls in the proposed DTC_SVPWM based induction motor drive system, thereby dramatically reducing the torque ripple. Then the controller based on space vector modulation is designed to be applied in the control of Induction Motor (IM) with a three-level Inverter. This type of Inverter has Several advantages over the standard Five-level CSI, such as a greater number of levels in the output voltage waveforms, Lower dv/dt, less harmonic distortion in voltage and current waveforms and lower switching frequencies Eliminated By SVPWM Tech. simulation results are reported to demonstrate its effectiveness. The entire control scheme is implemented with Matlab/Simulink.

Introduction

Direct torque control (DTC) has emerged as an alternative to field-oriented control (FOC) for high-performance ac drives, since it was first proposed in the mid-1980s .The merits of DTC can be summarized as fast torque response, simple structure (no need of complicated coordinate transformation, current regulation, or modulation block), and robustness against motor parameter variation. On the other hand, multilevel inverters have attracted considerable attention, especially in high-power application areas. The three-level neutral-point-clamped (NPC) inverter is one of the most commonly used multilevel inverter topologies in high-power ac drives. models [13], and precise offline wavelet-based feeder models [14]. For more accuracy, modeling of the high-frequency parasitic current paths [15], feeder insulation structure study [16], and time-varying equations [17] can be utilized. Frequency-domain analysis is a powerful tool in feeder modeling [18]. Lumped *L* and *C* elements can represent the feeder effectively, even for transient analysis. Applying this technique is simple and does not relatively scarify the accuracy [18], [19]; hence, this modeling technique is used in this paper. The long feeder connecting the motor with its associated drive makes a speed-sensor-based operation impractical; hence, a speed sensorless technique is prerequisite. There are many RECENT development in semiconductor devices and control strategies has enabled the use of variable speed drives (VSDs) in medium-voltage (MV) applications, such as electrical submersible pumps, ventilation fans, and underground mines where motor remote operation is mandatory [1]–[3].

The motor connection with a voltage source inverter (VSI)-based drive via a long feeder incurs many problems. Among them is the traveling wave phenomenon that causes doubling and ringing of the motor terminal voltage. These phenomena have adverse effects on motor insulation and contribute to bearing currents [4], [5], in addition to distorted common-mode voltage [6] and EMI problems [7].

Contrarily, the current source inverter (CSI) is a strong candidate for long motor feeder drives as it benefits from motor-friendly voltage waveforms which inhibit the traveling wave phenomena and hence do not stress motor insulation. In addition, the inherent short circuit proof operation and power reversal capabilities encouraged more exploitation into the CSI

Tele:

E-mail addresses: sravanthi_kuti@yahoo.com

integration in long motor feeder drives [1], [8], [9]. The basic system description is shown in Fig. 1.

Analysis of long motor feeder drives needs reliable modeling of the complete drive system, especially the feeder. Several techniques are proposed for feeder modeling, such as frequency-dependent models [10], on-line feeder parameter estimation [11], [12], frequency-dependent lumped segment closed-loop techniques used for induction motor speed estimation, such as the model reference adaptive system (MRAS) based on rotor flux [20], rotor flux derivative [21], [22], stator voltages [23], modified stator model [24], full-order observers [25], [26], reduced-order nonlinear observers [27], [28], Kalman filter observers [29], [30], or sliding mode observers [31], [32]. Other speed estimation techniques that do not rely on volt-age/current measurement include artificial intelligence such as neural networks [33], [34], harmonic rotor slotting [35], [36], or high-frequency signal injection [37], [38]. MRAS based on a rotor flux technique is simple, stable, and robust against ma-chine parameter variation. This method is selected for use in this paper.

The MRAS speed estimator requires motor voltages and cur-rents as inputs. Direct measurement of the motor voltages and currents is impractical for long motor feeder drives due to feeder length or safety/environmental precautions. Hence, the motor voltage and current must be calculated from the inverter side.

Another point that should be considered in the MRAS speed estimation practical implementation is as follows: dc offset occurs in the stator model. This offset occurs due to two reasons. First, dc offset occurs in the motor measurements due to dissimilar temperature coefficients of the measurement transducers in the three-phase motor lines [39], [40]. Second, flux estimation, using open-loop integrators, causes dc offset due to the uncertainty in the integration initial condition and the absence of integration limiters [40]. DC-offset problems result in a flux estimation error which affects the speed estimation accuracy. Hence, dc-offset problems need to be mitigated to enhance speed estimation accuracy.

Many approaches have been proposed to overcome the problem of dc offset in the stator model. Replacement of the integrator in the stator model with a low-pass filter usually dominates [20]. This introduces more delay and inaccuracy in the rotor flux phase angle estimation; thus, the use of the rotor flux derivative instead of the rotor flux is introduced [21], [22]. The main problem with using the rotor flux derivative is the generation of high-frequency components in the motor stator current that creates computational problems. Improved MRAS based on the rotor flux compensates the phase angle and amplitude errors of the low-pass filter, using a load-dependent flux observer [24] but the introduced second-order filter adds extra error to the estimated flux. Another proposed improvement uses a low-pass filter with corner frequencies that vary with the fundamental motor voltage frequency and compensates for the phase and amplitude error using their steady-state values [41]. The speed reversal problem associated with this technique is eliminated by performing the compensation before the low-pass filter [42]. Another way to improve the integration method is to force the flux trajectory to be circle by using an extra PI controller, thus eliminating dc offset [43]. This technique has good steady-state performance but exhibits start-up problems. Also, in the case of dc-offset distorted measured motor currents, keeping the flux in a circular trajectory does not pre-serve oscillations in the estimated speed as this method only affects the total flux vector. It does not solve the shift created in the flux $d - q$ components resulting from dc offset in the cur-rent measurement. High-performance operation, even near zero speed, is achieved by constructing three compensators [44]: first, feed-forward compensation for the large time constant drift due to dissimilar temperature coefficients in current measurement boards, by tracking the time variable dc-offset voltage using a parallel stator model; second, feedback compensation for the high-frequency components in flux $d - q$ components using a PI controller and the error between the reference and the estimated flux vectors; and third, compensation for the inverter nonlinear behavior and online resistance estimation for the motor. More-over, this method uses open-loop integration, thus benefiting from a wide estimation bandwidth. Despite these advantages, this method is relatively complex as it uses three compensation techniques. Another technique based on two resonant-type observers in addition to a conventional PI controller was presented [45], [46]. Operation near zero speed shows promising results but suffers from complexity. Moreover, this technique was presented for PMSM and not tested for induction motor drives. The advantage of the statically compensated voltage model lies in its simplicity, using only three integrators, one division, as well as a number of multiplications and additions/subtractions. This makes the design and implementation straightforward with limitations regarding frequency lockup instability [47].

In this paper, a modified dc-offset eliminator for improved flux estimation, needed for an MRAS speed estimation, is proposed. The presented dc-offset eliminator compensates the offsets due to the open-loop integrators in the MRAS stator model. The proposed eliminator offers single compensation core with simplified implementation in addition to wide bandwidth. Moreover, the errors resulting from motor current measurement are mitigated using a proposed dc-offset current measurement error compensator utilizing an effective adaptive high band-width algorithm. An experimental setup is implemented with a 1-km feeder model. Practical aspects, such as feeder selection and pulse width modulation (PWM) limitations, are considered in the experimental setup to match a scaled-down actual MV drive. Simulation in addition to experimental results verifies the effectiveness of the proposed system.

MRAS Speed Estimation

The application of MRAS in speed estimation can be achieved by constructing two models (observers) to estimate the rotor flux d–q components in the stationary reference frame [20]. The first observer, reference model, calculates the rotor flux d–q components in the stationary reference frame utilizing the motor voltages and currents as inputs. The second observer, adapted/adjusted model, calculates the rotor flux d–q components in the stationary reference frame utilizing the motor cur-rent and the estimated speed as inputs. The error from the cross multiplication of the stator and rotor model outputs is used to generate the estimated speed using a PI controller. Open-loop tuning is not preferred in MRAS speed estimation as the process does not have self-regulation. Moreover, instead of analytically adjusting PI controllers by using the frequency response method, the ultimate cycle-based Ziegler–Nichols tuning method is utilized [48]. The estimated speed is used as the adaptation signal for the rotor model. The ultimate cycle-based Ziegler–Nichols tuning method offers simple digital realization as well as straightforward tuning design steps, yet artificial intelligence-based sophisticated controllers such as adaptive controllers [51], neural network controllers [52], and fuzzy controllers [53] have been recently adopted for MRAS speed estimation but not considered in this paper. The system equations are as follows: 1)

stator model (reference model)

Sector of Flux→		1	2	3	4	5	6
C_ψ= 0	C_r=-1	$V_{2\text{-VSI}}$	$V_{3\text{-VSI}}$	$V_{4\text{-VSI}}$	$V_{5\text{-VSI}}$	$V_{6\text{-VSI}}$	$V_{1\text{-VSI}}$
	C_r= 0	$V_{7\text{-VSI}}$	$V_{0\text{-VSI}}$	$V_{7\text{-VSI}}$	$V_{0\text{-VSI}}$	$V_{7\text{-VSI}}$	$V_{0\text{-VSI}}$
	C_r= 1	$V_{6\text{-VSI}}$	$V_{1\text{-VSI}}$	$V_{2\text{-VSI}}$	$V_{3\text{-VSI}}$	$V_{4\text{-VSI}}$	$V_{5\text{-VSI}}$
C_ψ=+1	C_r=-1	$V_{3\text{-VSI}}$	$V_{4\text{-VSI}}$	$V_{5\text{-VSI}}$	$V_{6\text{-VSI}}$	$V_{1\text{-VSI}}$	$V_{2\text{-VSI}}$
	C_r= 0	$V_{0\text{-VSI}}$	$V_{7\text{-VSI}}$	$V_{0\text{-VSI}}$	$V_{7\text{-VSI}}$	$V_{0\text{-VSI}}$	$V_{7\text{-VSI}}$
	C_r= 1	$V_{5\text{-VSI}}$	$V_{6\text{-VSI}}$	$V_{1\text{-VSI}}$	$V_{2\text{-VSI}}$	$V_{3\text{-VSI}}$	$V_{4\text{-VSI}}$

Table. I. Basic DTC switching table

Conventional direct torque control

Mathematical mode of induction machine

Direct torque control system applies mathematical analysis about space vector. The mathematical mode of induction Machine is shown in"Fig. 1".

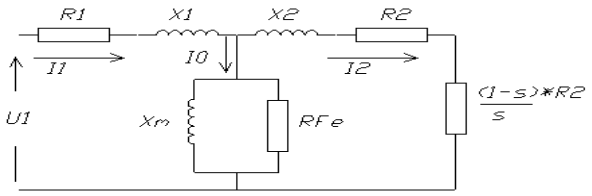

Fig. 1. Induction Motor Equavalent Block

According to "Fig. 1" flux–linkage equations of induction machines in the stator stationary reference frame as follows.

$\Psi_{\alpha s} = \int (v_{\alpha s} - R_s i_{\alpha s})\, dt$. (1)

$\Psi_{\beta s} = \int (v_{\beta s} - R_s i_{\beta s})\, dt$. (2)

$\Psi_a = \int (v_\beta)$ (3)

Where $\Psi_{\alpha s}$ and $\Psi_{\beta s}$ are the α-axis and β-axis component of $\bar{\psi}_s$ respectively; $v_{\alpha s}$ and $v_{\beta s}$ are the α -axis and β-axis component of $\bar{v}_s$ respectively; $i_{\alpha s}$ and $i_{\beta s}$ are the α-axis and β-axis component of $\bar{\imath}_s$ respectively.

The electromagnetic torque can be expressed using the following equation

Where T_e is electromagnetic torque and n_p is the number of rotor pole pairs.

Principle of direct torque control

The basic principle in conventional DTC for induction motors is to directly select stator voltage vectors by means of a hysteresis stator flux and torque control. As it is shown in" Fig. 2".

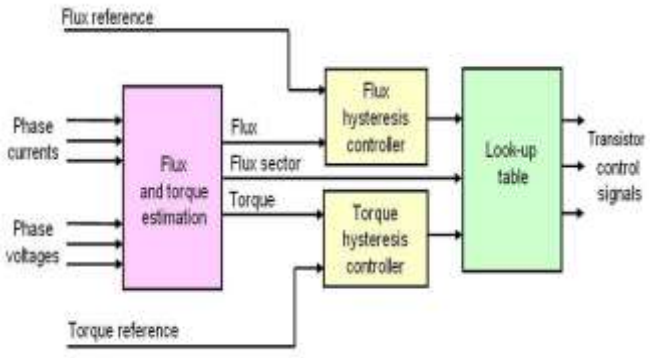

Fig.2.DTC Torque & Speed Estimation Block

From "Fig. 2" can obtain stator flux and torque references are compared with the corresponding estimated values. Both stator flux and torque errors, and, are processed by means of a hysteresis band comparators. In particular, stator flux is controlled by a two-level hysteresis comparator, whereas the torque is controlled by a three-level comparator. On the basis of the hysteresis comparators and stator flux sector a proper VSI voltage vector is selected by means of the switching table given in "Tab.I".

CSI-IM Structure With SVPWM Technique

The internal structure of the CSI-IM is shown in Fig. 2. It consists of three CSIs (CSI1, CSI2, and CSI3) which are connected back to back through a common dc-link capacitor. In the proposed configuration, CSI1 is connected in series with BUS1 and CSI2 is connected in parallel with load L1 at the end of Feeder1. CSI3 is connected in series with BUS2 at the Feeder2 end Each of the three CSIs in Fig. 2 is realized by a three-phase converter with a commutation reactor and high-pass output filter as shown in Fig. 3. The commutation reactor (L_f) and high-pass output filter (R_f, C_f) are connected to prevent the flow of switching harmonics into the power supply. Asshown in

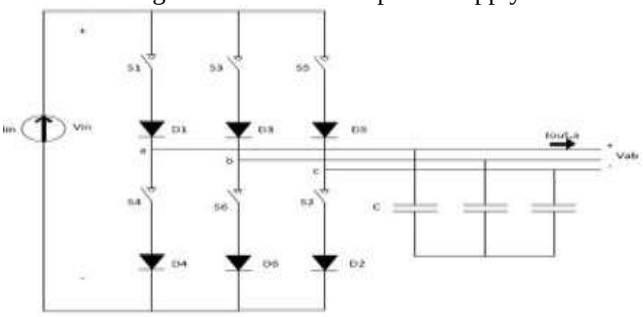

Fig.3 Schematic structure of a CSI

Fig. 2, all converters are supplied from a common dc-link Inductor and connected to the IM system through LCL Filters.:

1) To regulate the load voltage (u_{l1}) against sag/swell and disturbances in the system to protect the nonlinear/sensitive load L1;

2)To regulate the load Torque (u_{l2}) against disturbances in the system to protect the sensitive/critical load L2;

3)To compensate for the reactive and harmonic components of nonlinear IM load current (i_{l1})

DC-AC converter space vector modulation

6 power switches of inverter with 8 possible combinations shown in "Figure. 3" are corresponding to effective voltage space vector U_1 - U_6 and 2 zero vector U_0,U_7. The phase angle between one effective voltage space vector and adjacent one is 60 degrees. They constitute 6 uniform segments. The three digits in brackets express the linking state between three-phase output A,B,C and the input DC, such as M=101 which represents the switching of the switches S_{pA},S_{nB} and S_{pC}.

The output voltage space vectors and the corresponding switching states are represented in "Fig. 5".

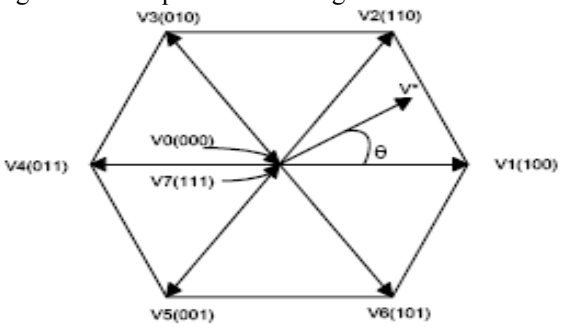

Fig.5,The composition of output voltage vector and Switching stages

Any expected output voltage space vector U_j is formed by adjacent two basic output voltage vectors U_M, U_N and zero output voltage U_0 or U_7. suppose the angle between U_j and U_N is θ_j .

$U_j = d_M U_M + d_N U_N + d_0 U_0$ (7)

Where d_M, d_N and d_0 are the ratio cycles of U_M, U_N and U_0 respectively. And

$$d_M = T_M/T_s = m_v \sin(60^0 - \theta_j) \quad (8)$$

$$d_N = T_N/T_s = m_v \sin(\theta_j) \quad (9)$$

$$d_0 = 1 - d_M - d_N \quad (10)$$

Where T_M, T_N is the switching time of vectors U_M and U_N respectively. T_s is the switching period of PWM. m_v is the modulation index of output voltage. And

$$m_v = (2/3)^{1/2} U_{om}/(U_{im} m_c \cos\emptyset) \quad (11)$$

Where U_{om} and U_{im} are the amplitude of output and input voltage, m_c is the input current modulation index, generally set $m_c = 1$. $\emptyset$ is the input power factor angle. When the rotating space vector U_j locates in a segment, the local average of output voltage can be formed by two adjacent basic voltage space vectors constituting this segment and one zero voltage space vector.

AC-DC converter space vector modulation

The space vector modulation process of AC-DC is completely similar to the modulation process of DC-AC. Its topology is represented in the left dotted line frame of "Fig. 4". The corresponding formulas are similar as well. After rectification, the DC voltage is.

$$U_d = 1.5 m_c U_{im} \cos\emptyset \quad (12)$$

DC-AC converter space vector modulation

Three-phase matrix converter module includes nine bidirectional switches as shown in "Fig. 3". There are 27 possible switching configurations (SCs), only 21 SCs can be used to implement the DTC algorithm for MC as shown in "Tab. II": group I (±1, ±2, …, ±9) consists of the SCs which have two output phases connected to the same one of the other input phase, group II (0a, 0b, 0c) consists of the SCs which have all output phases connected to a common input phase. For each SCs, the corresponding output line-to-neutral voltage vector and input line current vector have the fixed directions as represented in "Fig. 6".

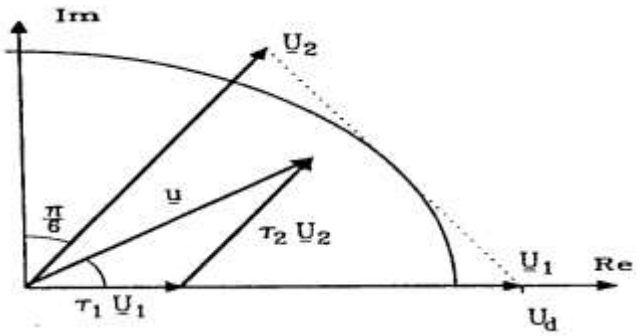

Fig 6.The line to newtral Voltage Vectors

The other 6 SCs have the output phases connected to the different input phases. In this case, the output voltage vector and input current vector have variable directions and cannot be usefully used.

Novel DTC-SVPWM use five level converter

The novel DTC-SVPWM method will apply the direct SVPWM technique to overcome the disadvantages of the conventional DTC for matrix converter [14],[15]. According to the input voltage line to neutral vector sector location, to combine the desired imaginary non-zero VSI voltage vector, the two non-zero voltage vectors will be selected. The criteria utilized to implement the switching patterns for the matrix converter can be explained referring to the following example.

We can assume the imaginary VSI voltage vector is V1, and the input voltage lint-to-neutral vector [12],[13] is located in sector 1 as shown in "Fig. 7" .

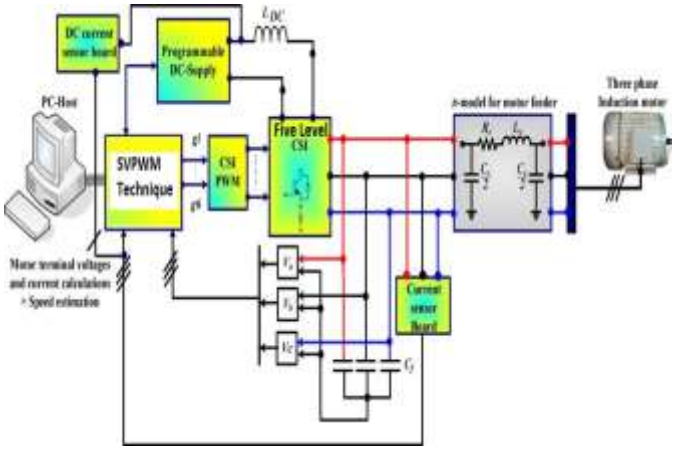

Fig 7. DTC_SVPWM IM with CSI Block

From "Tab. II", in order to generate a voltage vector in the same direction of V1, there are 6 possible SCs (□1, □2, □3). According to the input voltage vector location, there are only 3 SCs having the voltage vectors as same direction to V1: +1, -2 and -3. To synthesize the input current vector to be in phase with the input voltage vector located in sector 1, two SCs finally selected are +1 and -3. The switching table based on these criteria is shown in Fig.8.1

SVPWM PWM techniques

A different approach to SPWM is based on the space vector representation of voltages in the d, q plane. The d, q components are found by Park transform, where the total power, as well as the impedance, remains unchanged.

Fig: space vector shows 8 space vectors in according to 8 switching positions of inverter, V* is the phase-to-center voltage which is obtained by proper selection of adjacent vectors V1 and V2.

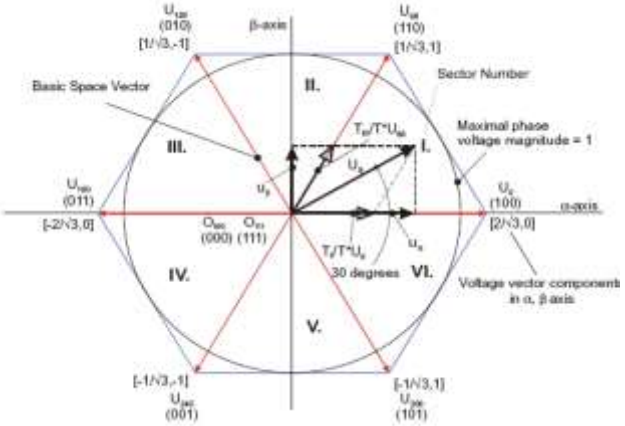

Fig 8. Inverter output voltage space vector

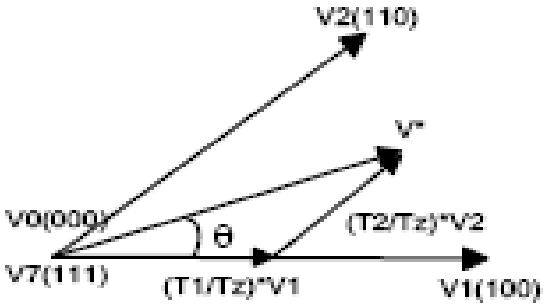

Fig 8.1 Determination of Switching times

The reference space vector V* is given by Equation (13), where T1, T2 are the intervals of application of vector V1 and V2 respectively, and zero vectors V0 and V7 are selected for T0.

V* Tz = V1 *T1 + V2 *T2 + V0 *(T0/2) + V7 *(T0/2)….(13)

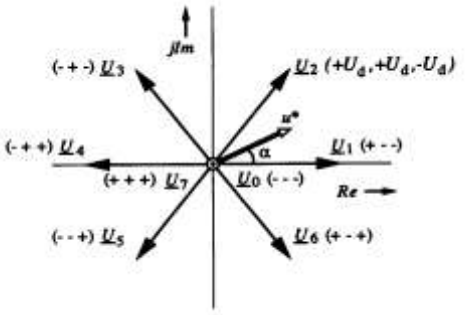

Fig 8.2 Space vector Modulation

The amplitude of u0 and u7 equals 0. The other vectors u1…u6 have the same amplitude and are 60 degrees shifted. By varying the relative on-switching time Tc of the different vectors, the space vector u* and also the output voltages ua, ub and uc can be varied and is defined as:

ua = Re (u*)

ub = Re (u* . a-1)

uc = Re (u* . a-2) ……(14)

During a switching period Tc and considering for example the first sector, the vectors u0, u1 and u2 will be switched on alternatively.

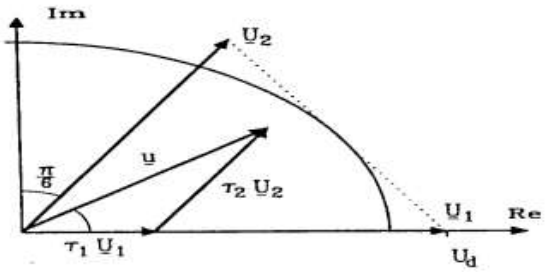

Fig.8.3 Definition of the Space vector

Depending on the switching times t0, t1 and t2 the space vector u* is defined as:

u* = 1/Tc . (t0 . u0 + t1 . u1 + t2 . u2)

u* = t0 . u0 + t1 . u1 + t2 . u2

u* = t1 . u1 + t2 . u2 …….. (15)

Where

t0 + t1 + t2 = Tc and

t0 + t1 + t2 = 1

t0, t1 and t2 are the relative values of the on witching times. They are defined as: t1 = m . cos (a + p/6) t2 = m . sin a t0 = 1 - t1 - t2

Their values are implemented in a table for a modulation factor m = 1. Then it will be easy to calculate the space vector u* and the output voltages ua, ub and uc. The voltage vector u* can be provided directly by the optimal vector control laws w1, v_{sa} and v_{sb}. In order to generate the phase voltages ua, ub and uc corresponding to the desired voltage vector u* the above SVPWM strategy is proposed

Simulation of DTC-SVPWM using MC

The simulation model of DTC-SVPWM using MC

In order to verify the behavior of the proposed scheme, some simulation has been carried out assuming a sampling period of 50µs. The system simulation model is shown in "Fig. 8". The machine utilized for simulations is a three-phase 3KW cage induction motor:

P_n=2.2kw,U_n=380V,

R_S=4.35Ω,Rr=0.43Ω,

L_s=2mH， L_r=2mH，

L_m=69.31mH，

J=0.089， P=2.

The whole system has been simulated using the Simulink package. Equation (5) and Equation (6) are used to obtain the matrix output voltages and the input currents respectively, thus assuming ideal switching devices. The mains filtered line current is calculated on the basis of the matrix input current.

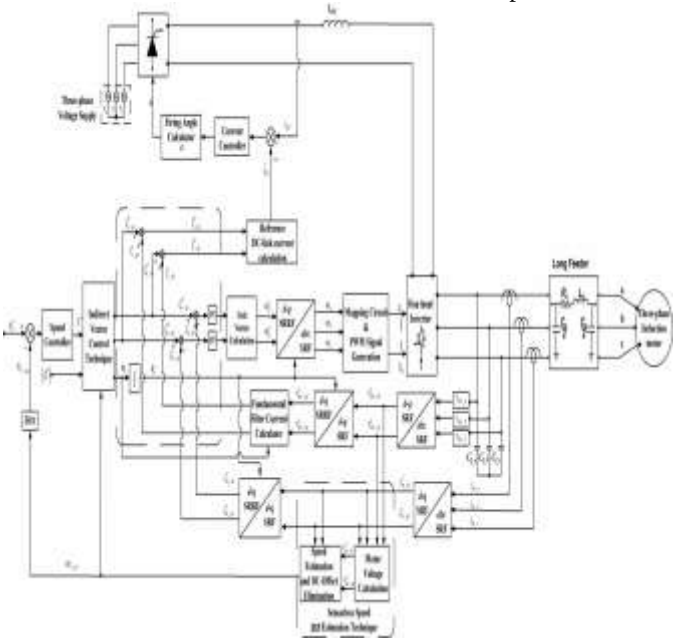

Fig.9.Simulation DTC_SVPWM_Multi Converter

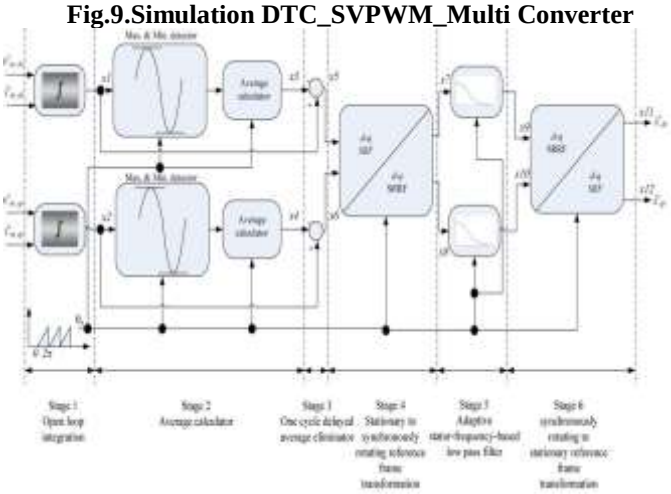

Fig 10. Simulation DTC_SVPWM_ SRF Control Block

The simulation result of DTC-SVPWM using MC

Both steady states at the high and low speed, the dynamic performance are shown to verify the effectiveness of the proposed MC-DTC method.

At the high speed operation, induction motor is running at speed 1000 rpm, rated load torque 25 Nm and flux reference 0.6 Wb. The simulation result show in "F. 9"-"Fig. 11".

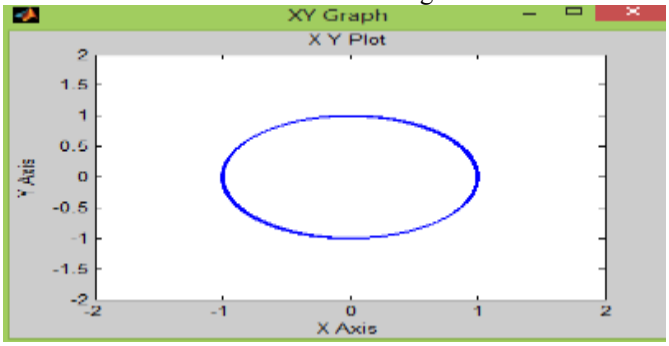

Fig.10.DQ Graph with SVPWM

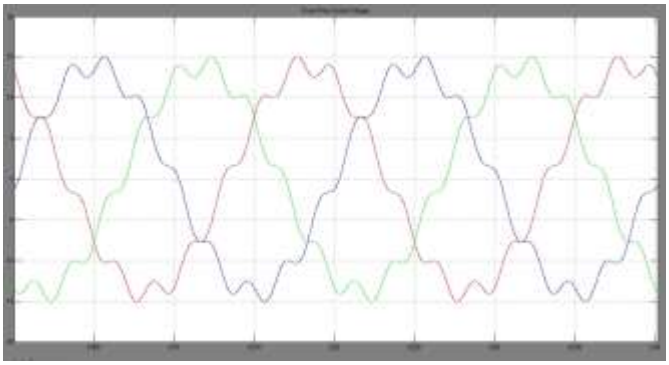

Fig.11 (a) Stator Current of IM with SVPWM technique

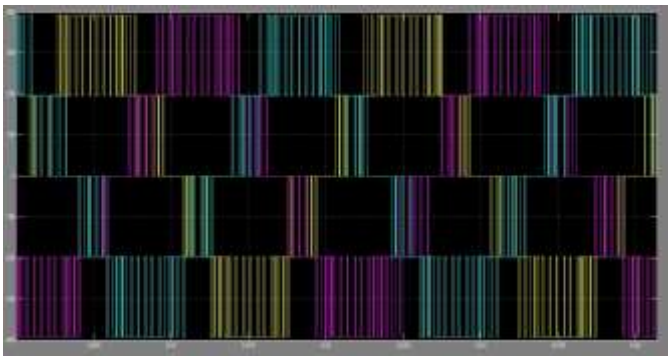

Fig.11 (b) Five Level Converter Voltage of IM with SVPWM technique

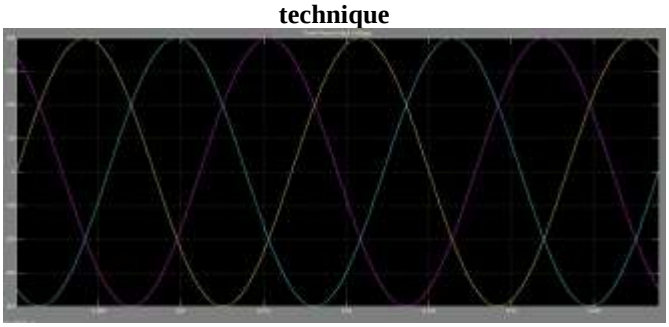

Fig.11 (c) Stator Voltage of IM with SVPWM technique

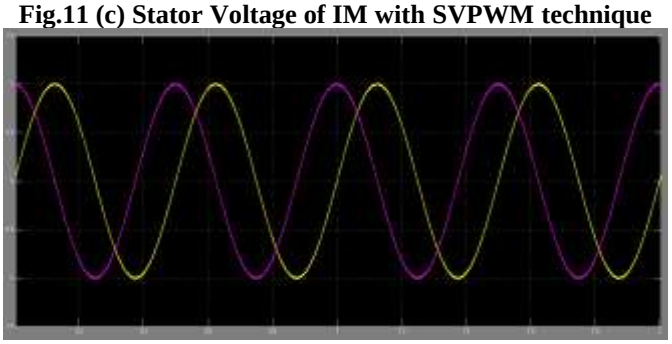

Fig.11 (d) DQ axis's of IM with SVPWM technique

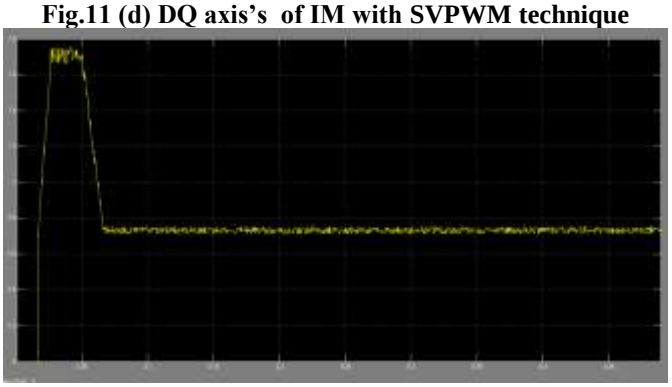

Fig.11 (e) Torque of IM with SVPWM technique

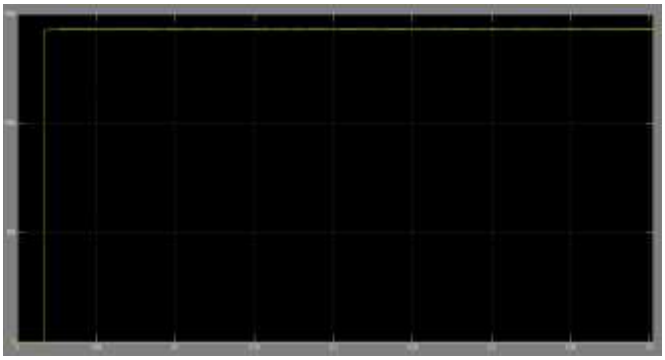

Fig.11 (f) Stator Voltage of IM with SVPWM technique

Fig.11.Simulation outputs graph for Stator current, MC voltage, torque and speed with DTC_SVPWM Five level converter for IM

Conclusion

This paper presents a new DTC-SVPWM method for Multi converter. The advantages of the DTC me have been successfully combined with the SVPWM method on Multi level converter. A new switching table for the DTC-SVPWM with Five Level Converter which fully controls the induction motor requirements is suggested, besides perfectly controlling the input unity power factor. The simulation results on the induction motor at the low and high speed range are shown to validate the effectiveness of the new control scheme. Furthermore, the novel control strategy shows the better input current harmonic spectrum and low-speed performance as compared to the conventional Five Level With SVPWM method and it can make the flux, Speed and torque small and stable. It has advantages and good future, it is worth further studying.

References

[1] Guo yougui, Zhu jianlin, "New modulaiton strategy on raising voltage transfer ratio for matrix converter," control theroy and applications,2006,23(4):542-546.

[2] Ding wei, Zhu jianlin, "Matrix congverter and its research situation," natural science journal of xiangtan university, 2002,24(2):185-187.

[3] Lan zhiyong, Zhu jianlin, "Simulation reearch of three phase to three phase sparse matrix converter," natural science journal of xiangtan university, 2005,27(3):110-115.

[4] CASDEI, D; SERRA, G; TANI, A; ZARRI, L. "Matrix Converter Modulation Strategies: A New General Approach on Space-Vector Representation of the Switch State", IEEE Trans. On Industrial Electronics, Vol. 49,No. 2, April 2002.

[5] CASDEI, D; SERRA, G; TANI, A. "The Use of Matrix Converters in Direct Torque Control of Induction Machines", IEEE Trans. On Industrial Electronics, Vol. 48, No. 6, December 2001.

[6] Romeo Ortega, Nikita Barabanov & Gerardo Escobar Valderrama, "Direct Torque Control of Induction Motors: Stability Analysis and Performance Improvement", IEEE transactions on automatic control, Vol. 46, No. 8, August 2001.

[7] TAKAHASHI, I; NOGUSHI, T. "A New Quick-Response and High-Efficiency Control Strategy of an Induction Motor", IEEE Trans. Industry Applications, Vol. 1A-22, pp 820-827, October 1986.

[8] DEPENBROCK, M. "Direct Self-Control (DSC) of Inverter-Fed Induction Machine", IEEE Trans. on Power Electronics, Vol. 3, No 4, pp 420-429, October 1988.

[9] LEE K B, BLAABGERG F, "improved direct torque control for sensorless matrix converter drives with constant switching frequency and torque ripple reduction", international journal of control, automation and system, 2006,4(1):113-123.

[10] C. Lascu, I. Boldea, and F. Blaabjerg, "Very-low-speed variable-structure control of sensorless induction machine drives without signal injection," IEEE Trans. Ind. Appl., vol. 41, no. 2, pp.591-598, Mar./Apr. 2005.
[11] C. Lascu, I. Boldea, and F. Blaabjerg, "Direct torque control of sensorless induction motor drives: a sliding-mode approach," IEEE Trans. Ind. Appl., vol. 40, no.2, pp.582-590, Mar/Apr. 2004
[12] Z. Xu and M. F. Rahman, "Direct torque and flux regulation of an IPM synchronous motor drive using variable structure control approach," IEEE Trans. Power Electron., vol.22, no. 6, pp.2487-2498, Nov. 2007.
[13] V. I. Utkin, "Sliding mode control design principles and applications to electric drives," IEEE Trans. Ind.Electron., vol.40, no. 1, pp.23-36, Feb. 203.
[14] C. Lascu and A. M. Traynadlowski, "Combining the principles of sliding mode, direct torque control, and space vector modulation in a high-performance sensorless AC drive," IEEE Trans. Ind. Appl., vol.40, no. 1, pp. 170-177, Jan./Feb. 2004.
[15] A. Naassani, E. Monmasson, and J. P. Louis, "Synthesis of direct torque and rotor flux control algorithms by means of sliding-mode theory," IEEE Trans. Ind.Electron., vol.52, no.3, pp. 785-799, June. 2005